

PROCEEDINGS OF SPIE

SPIDigitalLibrary.org/conference-proceedings-of-spie

Can optimised pulses improve the sensitivity of atom interferometers?

Saywell, Jack, Carey, Max, Dedes, Nikolaos, Kuprov, Ilya, Freearde, Tim

Jack Saywell, Max Carey, Nikolaos Dedes, Ilya Kuprov, Tim Freearde, "Can optimised pulses improve the sensitivity of atom interferometers?," Proc. SPIE 11881, Quantum Technology: Driving Commercialisation of an Enabling Science II, 118810R (6 October 2021); doi: 10.1117/12.2598991

SPIE.

Event: SPIE Photonex, 2021, Glasgow, Scotland, United Kingdom

Can optimised pulses improve the sensitivity of atom interferometers?

Jack Saywell^a, Max Carey^a, Nikolaos Dedes^a, Ilya Kuprov^b, and Tim Freegarde^a

^aSchool of Physics & Astronomy, University of Southampton, Southampton, SO17 1BJ, UK

^bSchool of Chemistry, University of Southampton, Southampton, SO17 1BJ, UK

ABSTRACT

The sensitivity of atom interferometers depends on the fidelity of the light pulses used as beamsplitters and mirrors. Atom interferometers typically employ pulses that affect $\pi/2$ and π fractional Rabi oscillations, the fidelities of which are reduced when there are variations in atomic velocity and laser intensity. We have previously demonstrated the application of optimal control theory to design pulses more robust to such errors; however, if these variations exhibit a time dependence over periods on the order of the interferometer duration then phase shifts can be introduced in the final fringe that potentially reduce the sensitivity. In this paper, we explain why care must be taken when optimising interferometer pulse sequences to ensure that phase shifts arising from inter-pulse variations are not significantly increased. We show that these phase shifts can in fact be minimised by choosing an appropriate measure of individual pulse fidelity.

Keywords: atom interferometry, optimal control theory, composite pulses

1. INTRODUCTION

Atom interferometric sensors^{1,2} - once confined to stable laboratory environments - are being adapted for use as portable devices with a wide range of applications from navigation to civil engineering.³ However, in order to reach their potential maximum sensitivity as mobile accelerometers, gyroscopes, and gravity gradiometers, they must be made more robust to noisy inhomogeneous environments.

Atom interferometers rely upon the diffraction and interference of atomic matter-waves,⁴ often by precisely-timed pulses of laser light. Raman transitions^{1,5,6} between two ground hyperfine levels in alkali-metal atoms are a popular diffraction mechanism in portable sensor designs,⁷⁻⁹ where fractional Rabi oscillations between the two states act as the beamsplitter ($\pi/2$) and mirror (π) operations.

These laser pulses must have high fidelity: if all atoms in the interferometer do not respond to the pulse in the same way, the measurement sensitivity will be reduced. Variations in resonance frequency (e.g. due to the non-zero atomic temperature) and variations in Rabi frequency (e.g. due to laser intensity gradients) lower the pulse fidelity.¹⁰ The result is a reduction in the fringe contrast and the introduction of unwanted phase shifts.¹¹

Replacing the $\pi/2$ and π pulses of constant laser intensity and phase with those in which the phase and intensity vary in time can mitigate the effect of these inhomogeneities. Quantum optimal control algorithms,^{12,13} many of which were developed in the field of nuclear magnetic resonance (NMR) to compensate errors in the control of nuclear spins using radio-frequency fields, can be adapted to optimise shaped pulses that perform interferometry operations in the presence of control errors. Although the principles of robust pulse design in atom interferometry and NMR are similar, the objectives and specific control errors - including their physical origin, time dependence and the correlations between them - are different.

We have previously adapted optimal control to the design of individual Raman pulses for atom interferometry.¹⁴⁻¹⁶ These pulses were designed to be robust to large variations in Rabi frequency and detuning. In this paper, we investigate whether these optimised pulses can minimise phase shifts caused when there is a variation in detuning and/or Rabi frequency between the pulses in a 3-pulse Mach-Zehnder interferometer. We first explain how variation in these quantities causes phase shifts when using conventional $\pi/2$ and π pulses and then explain how optimal control can be used to design pulses which minimise these unwanted shifts.

Further author information: (Send correspondence to J.S.)

J.S.: E-mail: j.c.saywell@soton.ac.uk

Quantum Technology: Driving Commercialisation of an Enabling Science II, edited by Miles J. Padgett, Kai Bongs, Alessandro Fedrizzi, Alberto Politi, Proc. of SPIE Vol. 11881, 118810R
© 2021 SPIE · CCC code: 0277-786X/21/\$21 · doi: 10.1117/12.2598991

2. RAMAN PULSE THEORY

In a Raman transition,⁵ two counter-propagating laser beams with frequencies $\omega_1 = ck_1$ and $\omega_2 = ck_2$ couple two ground hyperfine levels $|g\rangle$ and $|e\rangle$ with hyperfine splitting ω_{eg} . Each laser is individually detuned from an upper intermediate level which is never significantly populated, resulting in a stable two-state system. Fractional Rabi oscillations between these two states may then be used to form beamsplitter and mirror operations in an atom interferometer. The atomic species assumed in this work is ⁸⁵Rb, and the specific levels used are $|g\rangle = |5S_{1/2}, F = 2\rangle$ and $|e\rangle = |5S_{1/2}, F = 3\rangle$, where $\omega_{eg} \approx 3\text{GHz}$. However, the following theory remains very general.

Neglecting the atomic momentum, we write the general state of our atom as $|\psi(t)\rangle = c_g(t)|g\rangle + c_e(t)|e\rangle$. The propagator that evolves an initial state under a Raman pulse of constant Rabi frequency Ω_R and relative laser phase ϕ_L and duration τ is given by¹⁷

$$\hat{U} = \begin{pmatrix} C^* & -iS^* \\ -iS & C \end{pmatrix}, \quad (1)$$

where C and S are defined as:

$$C \equiv \cos\left(\frac{\sqrt{\Omega_R^2 + \delta^2}(\tau)}{2}\right) + i\left(\frac{\delta}{\sqrt{\Omega_R^2 + \delta^2}}\right) \sin\left(\frac{\sqrt{\Omega_R^2 + \delta^2}(\tau)}{2}\right), \quad (2)$$

$$S \equiv e^{i\phi_L} \left(\frac{\Omega_R}{\sqrt{\Omega_R^2 + \delta^2}}\right) \sin\left(\frac{\sqrt{\Omega_R^2 + \delta^2}(\tau)}{2}\right). \quad (3)$$

δ is the two-photon Raman detuning, which is given by $\delta \equiv \delta_L - k_{\text{eff}}v - \hbar k_{\text{eff}}^2/(2m)$ and defines the resonance condition for the transition. $k_{\text{eff}} \equiv k_1 + k_2$ is the effective wave-number of the Raman transition, v is the component of the atomic velocity in the direction of the Raman beams, and m is the atomic mass. $\delta_L \equiv \omega_1 - \omega_2 - \omega_{eg}$ represents the frequency difference between the two lasers and the hyperfine splitting between $|g\rangle$ and $|e\rangle$. Throughout this paper, we assume δ is constant during a pulse.

The action of the Raman pulse propagator is equivalent to a rotation of the quantum state in the Bloch sphere picture.¹⁸ The axis of this rotation - known as the field vector - is given by

$$\mathbf{\Omega} = \Omega_R \cos(\phi_L)\mathbf{x} + \Omega_R \sin(\phi_L)\mathbf{y} + (\delta)\mathbf{z}, \quad (4)$$

and the rotation angle is given by

$$|\mathbf{\Omega}| \times \tau = \sqrt{\Omega_R^2 + \delta^2} \times \tau. \quad (5)$$

We define the effective Rabi frequency Ω_{eff} such that a constant-intensity pulse of duration π/Ω_{eff} or $\pi/2\Omega_{\text{eff}}$ performs a π or $\pi/2$ rotation if $\Omega_R = \Omega_{\text{eff}}$. These are referred to as “rectangular” $\pi/2$ and π pulses.

Non-zero detunings shift the rotation axis from the equatorial plane, leading to a divergence in the resulting state trajectory, while variations in the Rabi frequency change the rotation angle. In the presence of these errors, termed “off-resonance” and “pulse-length”,¹⁰ respectively, the fidelity of $\pi/2$ and π pulses is reduced.

In the case of no off-resonance or pulse-length error ($\delta = 0$ and $\Omega_R = \Omega_{\text{eff}}$), we obtain the following error-free propagators for the $\pi/2$ and π pulses:

$$\hat{U}_{\pi/2} = \begin{pmatrix} \frac{\sqrt{2}}{2} & -ie^{-i\phi_L} \frac{\sqrt{2}}{2} \\ -ie^{i\phi_L} \frac{\sqrt{2}}{2} & \frac{\sqrt{2}}{2} \end{pmatrix}, \quad (6)$$

$$\hat{U}_{\pi} = \begin{pmatrix} 0 & -ie^{-i\phi_L} \\ -ie^{i\phi_L} & 0 \end{pmatrix}. \quad (7)$$

3. PHASE SHIFTS DUE TO IMPERFECT RECTANGULAR PULSES

In this section we explain how variations in detuning and Rabi frequency between the three pulses in the Mach-Zehnder interferometer lead to phase shifts in the interferometer fringe. We label the three consecutive pulses in the $\pi/2 - \pi - \pi/2$ sequence by 1, 2, and 3.

For an atom initially in the state $|g\rangle$, the probability for it to exit the interferometer in the state $|e\rangle$ is given by

$$P_e = \frac{A}{2} - \frac{B}{2} \cos(\Phi + \Delta\Phi), \quad (8)$$

where A is the fringe offset, B is the contrast, Φ is the inertial phase shift - defined as the difference between the phases accumulated in each period of free evolution - and $\Delta\Phi$ is a phase shift contribution from the pulses themselves. By following the argument given by Stoner *et al.*¹⁷ and multiplying together the individual propagators for the three pulses and the two periods of free-evolution between them, we find the following expressions for A , B , and $\Delta\Phi$:

$$A = 2(|S_1|^2|S_2|^2|S_3|^2 + |C_1|^2|S_2|^2|C_3|^2 + |S_1|^2|C_2|^2|C_3|^2 + |C_1|^2|C_2|^2|S_3|^2) \quad (9)$$

$$B = 4|C_1||S_1||S_2|^2|C_3||S_3| \quad (10)$$

$$\Delta\Phi = \phi(C_1) + \phi(S_1) - 2\phi(S_2) + \phi(S_3) - \phi(C_3) \quad (11)$$

$$\equiv \phi_1 + \phi_2 + \phi_3. \quad (12)$$

We have used the notation $\phi(A)$ to indicate the argument of the complex number A , and collected the phase contributions from each pulse by defining $\phi_1 \equiv \phi(C_1) + \phi(S_1)$, $\phi_2 \equiv -2\phi(S_2)$, and $\phi_3 \equiv \phi(S_3) - \phi(C_3)$. For the ideal propagators (Equations 6 and 7), A becomes 1, B becomes 1 and $\Delta\Phi = \phi_{L1} - 2\phi_{L2} + \phi_{L3}$ (the constant laser phases during each pulse). For ideal pulses, each atom exits the interferometer with the same phase shift and the thermally averaged contrast will be maximised. We find the following individual conditions on C_i and S_i for ideal pulses:

$$|C_i|^2 = \begin{cases} 1/2, & i = 1, 3 \\ 0, & i = 2 \end{cases} \quad (13)$$

$$|S_i|^2 = \begin{cases} 1/2, & i = 1, 3 \\ 1, & i = 2. \end{cases} \quad (14)$$

When there are variations in Rabi frequency and detuning, the contrast B decreases and the offset A varies from its ideal value of 1. However, if the first pulse (the beamsplitter) produces an equal superposition of $|g\rangle$ and $|e\rangle$ ($|S_1|^2 = |C_1|^2 = 1/2$), then the offset is 1 even if the final two pulses are imperfect. The beamsplitter therefore sets the midpoint of the fringe.

The contribution of the π mirror pulse to the phase shift $\Delta\Phi$ is independent of δ and Ω_R , but the contributions of the beamsplitter and recombiner pulses are not. For example, in the case where $\phi_{L1} = \phi_{L3} = 0$ (resonant rotations about the x -axis), we find that¹¹

$$\phi_1 = \phi \left[\cos \left(\frac{\sqrt{\Omega_R^2 + \delta^2}(\tau)}{2} \right) + i \left(\frac{\delta}{\sqrt{\Omega_R^2 + \delta^2}} \right) \sin \left(\frac{\sqrt{\Omega_R^2 + \delta^2}(\tau)}{2} \right) \right], \quad (15)$$

$$\phi_3 = -\phi \left[\cos \left(\frac{\sqrt{\Omega_R^2 + \delta^2}(\tau)}{2} \right) + i \left(\frac{\delta}{\sqrt{\Omega_R^2 + \delta^2}} \right) \sin \left(\frac{\sqrt{\Omega_R^2 + \delta^2}(\tau)}{2} \right) \right]. \quad (16)$$

In Figure 1 a), we show ϕ_1 and ϕ_3 as functions of the detuning during each pulse. In terms of the Bloch sphere picture, $\phi_1 + \pi/2$ is the equatorial angle between the state vector and the x -axis. Although this angle depends on the detuning and Rabi frequency during the pulse, if there is no change in detuning or Rabi frequency between pulses 1 and 3, the phase contributions from each pulse will be equal and opposite and there will be no net change to $\Delta\Phi$.

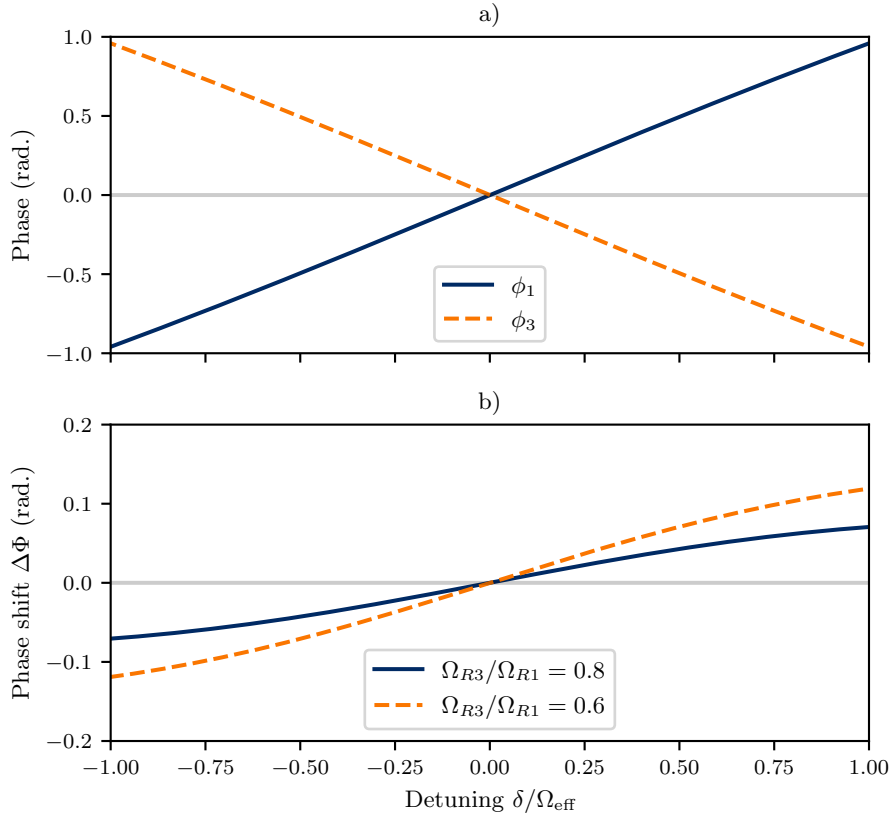


Figure 1. a) Simulated contributions to the interferometer phase from the first and final $\pi/2$ pulses in the sequence. ϕ_1 represents the relative phase of the superposition created by the first $\pi/2$ pulse. The Rabi frequency for each pulse was taken to be $\Omega_R = \Omega_{\text{eff}} = 200$ kHz. In b) we depict the total interferometer phase shift resulting from different Rabi frequencies between the first and final $\pi/2$ pulses. In this case, δ was assumed to be constant throughout the sequence and the effective Rabi frequency (equal to Ω_{R1}) was 200 kHz.

3.1 Phase shift due to change in detuning between pulses

As shown in Figure 1 a), the phase of the superposition state produced by the $\pi/2$ beamsplitter depends on the detuning during the pulse. Consequently, if the detuning changes between pulses 1 and 3, this shift will not be fully compensated by the final pulse and there will be a phase shift in the fringe. As an example, we consider the case of an interferometer measuring a constant acceleration a along the Raman beam axis. In this scenario, the inertial phase shift becomes $\Phi = k_{\text{eff}}aT^2$, where T is the dwell time between the pulses. If a or T is large enough, the change in detuning ($2k_{\text{eff}}aT$) between pulses 1 and 3 must be compensated by chirping the laser frequency difference at a rate that matches the acceleration.¹ If the chirp exactly cancels the acceleration, there will be no inertial phase shift. However, if there is a difference between the chirp and the acceleration, the detuning will be different between pulses and we expect an additional contribution to $\Delta\Phi$ from imperfect cancellation between ϕ_1 and ϕ_3 .¹⁷ There will also be a smaller contribution from the change in detuning occurring during each of the three pulses themselves, but we neglect this in this treatment.

3.2 Phase shift due to change in Rabi frequency between pulses

As the atom cloud expands throughout the interferometer sequence, a given atom will likely experience a different Rabi frequency throughout the pulse sequence. The size of this difference will depend on the width of the (typically Gaussian) laser beams, the atomic velocity (sampled from the temperature distribution), and the

duration of expansion. In this situation $\phi_1 + \phi_3$ results in a residual phase shift that depends on δ , and the ratio between Ω_{R1} and Ω_{R3} . This effect was studied in detail by Gillot *et al.*¹¹

We have, in Figure 1 b), depicted $\phi_1 + \phi_3$ as a function of a constant detuning δ for two different ratios of Ω_{R1}/Ω_{R3} . As noted by Gillot *et al.*,¹¹ this phase shift is antisymmetric as a function of δ , meaning that there is no average shift in the measured fringe if the laser detuning is exactly matched to the center of the velocity distribution and the velocity distribution is symmetric. This is because the measured fringe represents an average taken over the atomic velocity distribution.

4. OPTIMAL CONTROL THEORY

Optimal control theory¹³ may be used to obtain tailored Raman pulses where the relative laser phase and/or two-photon Rabi frequency Ω_R are varied in time to maximise a carefully chosen measure of pulse fidelity, for example to replace the beamsplitter and mirror pulses. We have previously optimised Raman pulses to increase interferometer contrast by engineering robustness to pulse-length and off-resonance errors.^{14–16} The pulse optimisation procedure relies on the open-loop NMR GRAdient Ascent Pulse Engineering (GRAPE) algorithm,^{12,19,20} and is implemented using the *Spinach* software toolbox.²¹

In our optimal control approach, we restrict our optimisation to piecewise constant waveforms, where Ω_R and/or ϕ_L may vary from step-to-step. We refer to $\Omega_R(t)$ and $\phi_L(t)$ as the amplitude and phase profiles of the pulse, respectively. The total duration of the pulse and the number of time-steps are chosen at the outset along with a guess (or random starting shape) for the waveform. We choose a fidelity measure that captures what we want the optimised pulse to do for an individual atom (e.g. perform a beamsplitter or mirror operation), and then iteratively update our guess using GRAPE until we find a sufficiently good pulse.

By averaging our fidelity measure over a range of pulse-length and/or off-resonance errors we may ensure a robust solution. The specific range of errors included in this ensemble determines the degree of error compensation provided by the optimised pulse although there are limits on performance which are mainly set by the pulse duration and maximum Rabi frequency.^{22,23} Penalties may also be applied to enforce smooth pulse shapes and limit the maximum Rabi frequency during the optimisation.

Since each optimised pulse has a piecewise constant Hamiltonian, the propagator for an individual step takes the same form as Equation 1 with C and S defined according to Equations 2 and 3. The total propagator for each pulse (\hat{U}_i , $i = 1, 2, 3$) is given by the time-ordered product of the propagators for each step and may still be written in the form of Equation 1. However, C and S for the total propagator are no longer given by Equations 2 and 3, and must be evaluated numerically.

5. PHASE SHIFTS DUE TO OPTIMISED PULSES

5.1 Pulse fidelity

Examining the interferometer output (Equation 8) allows us to define fidelities for each pulse. These fidelities reflect the role that each pulse plays in the Mach-Zehnder sequence. For example, the beamsplitter must prepare an equal superposition with constant relative phase and the mirror pulse must swap the two arms of the interferometer while preserving their relative phase. The beamsplitter acts on atoms all in the same initial state and can be thought of as a “point-to-point” operation.²² The mirror pulse, however, must correctly transform any initial superposition state, performing what can be described as a “universal-rotation”.²³

In our previous work,¹⁵ we presented the following fidelities for the beamsplitter and mirror pulses, defining a target state $|\psi_T\rangle = (|g\rangle + e^{i\phi_T}|e\rangle)/\sqrt{2}$ with target superposition phase ϕ_T for the beamsplitter and a target propagator $\hat{U}_T = \hat{U}_\pi$ for the mirror:

$$\mathcal{F}_1 = |\langle \psi_T | \hat{U}_1 | g \rangle|^2, \quad (17)$$

$$\mathcal{F}_2 = \frac{1}{2} \text{Tr}(\hat{U}_T^\dagger \hat{U}_2). \quad (18)$$

It can be shown²⁴ that maximising these two fidelities for a range of detunings and Rabi frequencies will yield pulses which satisfy the conditions in Equations 13 and 14 and minimise variation in phases ϕ_1 and ϕ_2 .

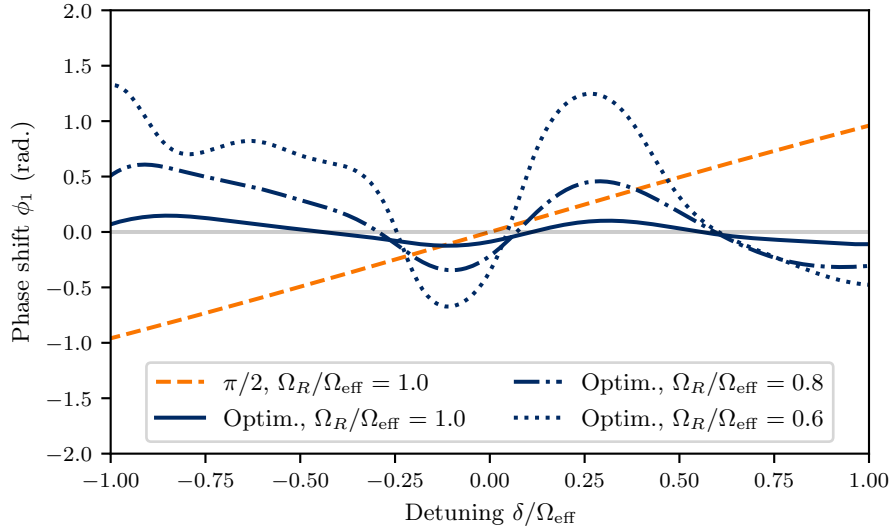


Figure 2. The phase contribution ϕ_1 of the optimised beamsplitter from Saywell *et al.*¹⁵ as a function of a constant detuning δ for $\Omega_R = \Omega_{\text{eff}} = 200$ kHz, $\Omega_R = 0.8 \times \Omega_{\text{eff}}$, and $\Omega_R = 0.6 \times \Omega_{\text{eff}}$. The same phase is also shown for a $\pi/2$ pulse. While the optimised pulse exhibits noticeable variations in ϕ_1 over the design range of detuning, combining pulses in a “flip-reversed” sequence means that the total phase contribution from the pulses cancels when the Rabi frequency is constant. However, variations in Rabi frequency between pulses negate this cancellation, and the large variations can then prove detrimental to the final signal.

For the final pulse, which must perform a phase-sensitive $\pi/2$ rotation about a fixed equatorial axis for any initial superposition state, we could optimise a universal-rotation by defining a target propagator $\hat{U}_T = \hat{U}_{\pi/2}$. However, this fidelity is actually more restrictive than necessary as only the z -component of the Bloch vector matters at the end of the interferometer: it need not be a universal-rotation. Instead, we obtain the final pulse, \hat{U}_3 , by time-reversing and phase-inverting the first pulse found by maximising \mathcal{F}_1 .¹⁵ If we apply this transformation, we find that²⁴

$$|C_3|, |S_3| = |C_1|, |S_1| \quad (19)$$

$$\phi(C_3) = \phi(C_1) \quad (20)$$

$$\phi(S_3) = -\phi(S_1), \quad (21)$$

thus satisfying the requirements on the final pulse. Using this construction procedure - which we refer to as “flip-reverse” for brevity - we also notice that $\Delta\Phi$ is independent of δ and Ω_R if these do not change throughout the sequence, meaning that any phase shift introduced by the first pulse will be cancelled by the final one.

Optimising pulses 1, 2, and 3 in the way described in this section yields solutions where variation in phases ϕ_1 , ϕ_2 , and ϕ_3 can be minimised within the optimisation error ensemble. However, if the final fidelity is less than unity, the phases can still vary with δ and Ω_R . Furthermore, these phases will remain unconstrained for detunings and Rabi frequencies outside the error ensemble.

Unlike the rectangular π mirror pulse, optimised mirror pulses will in general result in a phase contribution to the interferometer that varies with δ and Ω_R .¹⁴ This variation can be minimised within the error ensemble; however, if the mirror pulse is constrained to have a time-symmetric amplitude profile and a time-antisymmetric phase profile, then the contribution ϕ_2 becomes independent of δ and Ω_R .^{15,24}

5.2 Minimising phase shifts due to a change in Rabi frequency and detuning between the pulses

We have discussed how appropriate fidelity choices can minimise variations in the phases ϕ_1 , ϕ_2 , and ϕ_3 and how antisymmetric mirror pulses make ϕ_2 independent of the detuning and Rabi frequency during the pulse. In this

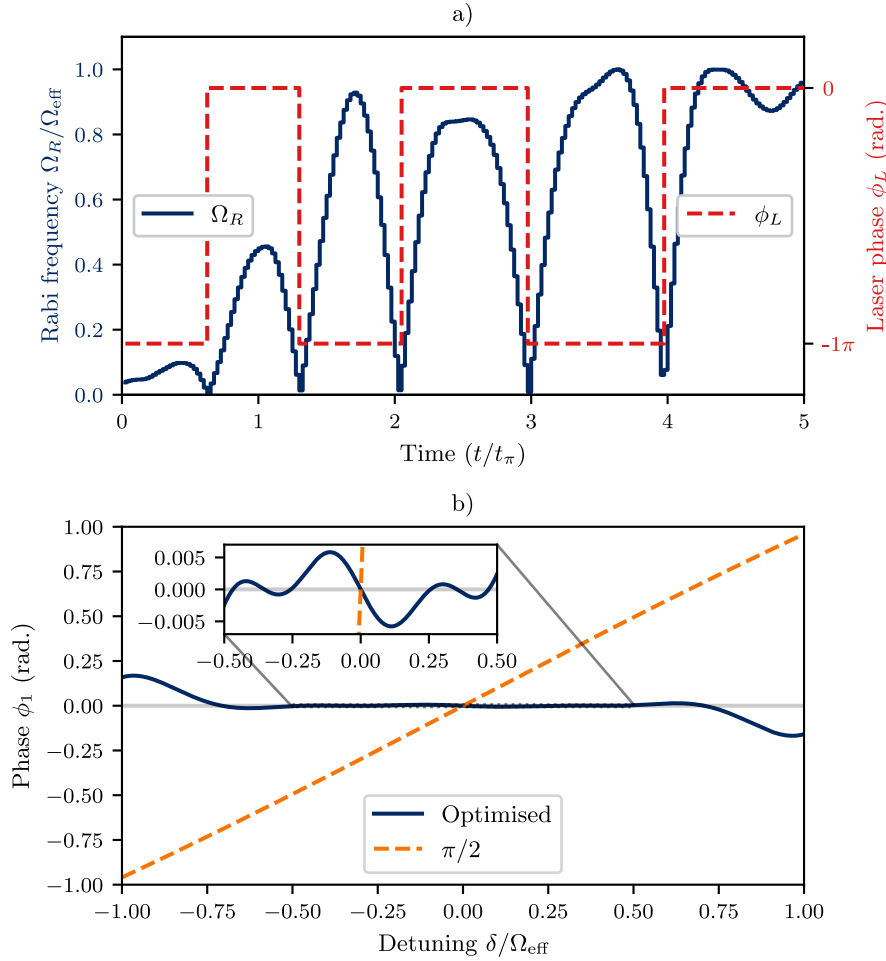


Figure 3. a) Laser phase and amplitude profiles for an optimised beamsplitter designed to be robust to variations in detuning in the range $-0.5 \times \Omega_{\text{eff}} < \delta < 0.5 \times \Omega_{\text{eff}}$ where $\Omega_{\text{eff}} = 200$ kHz. The laser phase was limited to $n\pi$ during the pulse where n is an integer. b) shows the superposition phase ϕ_1 produced by this optimised pulse as a function of a constant detuning δ . The same phase is shown for a $\pi/2$ pulse. We can see that the optimised pulse minimises variation in ϕ_1 over the design range of detuning. A constant phase shift has been applied to the optimised phase curve to aid visual comparison.

section we provide an example of an optimised beamsplitter and “flip-reverse” recombiner pulse which minimise the phase shifts caused by variation in δ and Ω_R between the pulses.

In Figure 2 we show the phase contribution ϕ_1 from the optimised beamsplitter presented in Saywell *et al.*,¹⁵ as a function of a constant detuning δ . The pulse was obtained by averaging the fidelity from Equation (17) over a range of detunings and Rabi frequencies. While the phase contribution is minimised over the optimisation range, there are noticeable fluctuations. The “flip-reverse” concatenation ensures that these variations cancel in a full interferometer sequence, but only if the Rabi frequency is constant. Significant variations in Rabi frequency between pulses would negate this cancellation, making the fluctuations in phase problematic by reducing signal contrast and/or introducing interferometer bias.

In Figure 3 a) we show the phase and amplitude profiles for a new beamsplitter pulse. This pulse was optimised using fidelity \mathcal{F}_1 with a target superposition phase of $-\pi/2$ averaged over a range of detunings ($-0.5 \times \Omega_{\text{eff}} < \delta < 0.5 \times \Omega_{\text{eff}}$) where the maximum Rabi frequency was limited to $\Omega_{\text{eff}} = 200$ kHz. We also

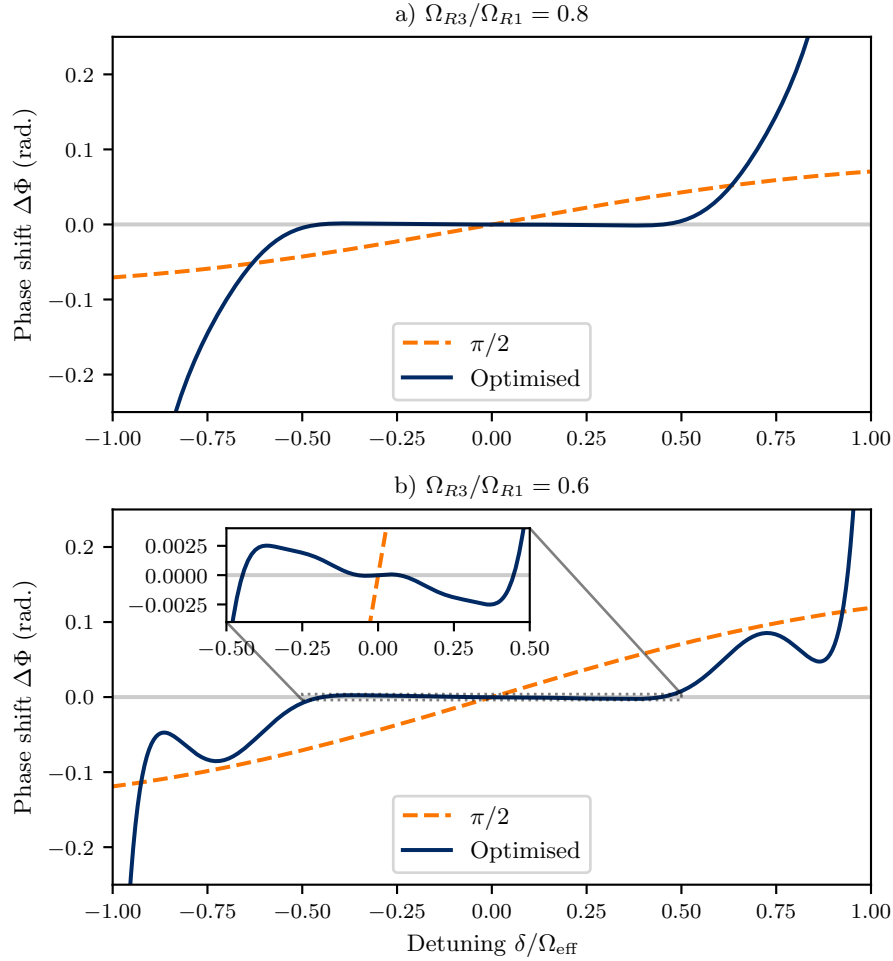


Figure 4. a) and b) depict the simulated contribution to the interferometer phase from pulses 1 and 3 when the Rabi frequency is decreased between the pulses. In a) $\Omega_{R3} = 0.8 \times \Omega_{R1}$ and in b) $\Omega_{R3} = 0.6 \times \Omega_{R1}$. The Rabi frequency for the first pulse Ω_{R1} was taken to be 200 kHz. We observe that the optimised beamsplitter and recombiner pulses are robust to this variation, minimising the shift in phase produced by rectangular $\pi/2$ pulses. A constant phase shift has been applied to the optimised phase curves to aid visual comparison.

minimised variation in the superposition phase ϕ_1 over this detuning ensemble for a range of Rabi frequencies ($0.6 \times \Omega_{\text{eff}} < \Omega_R < \Omega_{\text{eff}}$), to accommodate a possible decrease in Rabi frequency due to expansion of the atom cloud across a Gaussian beam. This was done by adapting the fidelity presented in Skinner *et al.*²⁵ to minimise only the x -component of the final Bloch vector over the error ensemble. Furthermore, the laser phase of this pulse was limited to integer multiples of π . This ensures that the phase ϕ_1 is anti-symmetric with respect to detuning.

The duration of the pulse was fixed at $5t_\pi$ (t_π is the duration of a π pulse at the effective Rabi frequency Ω_{eff}) with 200 time-steps. The phase ϕ_1 is shown as a function of detuning during the pulse in Figure 3 b) and compared with a $\pi/2$ pulse. We see that the phase is minimised over the optimisation region in detuning and that although this pulse is 10 times longer than the $\pi/2$ pulse, the shift due to a change in detuning between pulses 1 and 3 will be reduced.

In Figure 4, we show the contribution $\phi_1 + \phi_3$ to the interferometer phase as a function of detuning as the Rabi frequency is varied between pulse 1 and 3. We observe that the optimised beamsplitter and recombiner pulses

minimise the phase shift present when using $\pi/2$ pulses, reducing the sensitivity to detuning near resonance. In the case where $\Omega_{R3} = 0.6 \times \Omega_{R1}$ (Figure 4 b)), the magnitude of the phase shift at $\delta = 0.2 \times \Omega_{\text{eff}}$ is reduced from 29.9 mrad to 1.5 mrad by the optimised pulses.

6. DISCUSSION

In this paper we have discussed how, when employing shaped pulses found using optimal control in atom interferometers, care must be taken to minimise phase shifts that arise when the detuning and Rabi frequency vary between the pulses. We have explained how different fidelity measures and symmetry properties affect these phase shifts, and presented examples of optimised beamsplitter and recombiner pulses where the phase shifts caused by conventional $\pi/2$ pulses are reduced.

Employing frequency-swept adiabatic pulses as beamsplitters and recombiners is another possible way to reduce the phase errors discussed in this paper.²⁶ The superposition phase produced by an adiabatic half-passage pulse is - in the adiabatic limit - highly robust to variations in the Rabi frequency during the pulse. However, adiabatic beamsplitters are significantly longer than $\pi/2$ pulses and produce equal superpositions only for a narrow range of detunings.

The optimised pulses discussed in this paper require accurate and precise experimental control of the Raman beam intensities and relative laser phase. If the optimised waveforms are distorted by errors in the experimental phase and intensity modulation, then the pulses “seen” by the atoms will not match the optimised waveforms and the effective fidelities will be reduced. In practice, therefore, applying optimised pulses requires careful experimental calibration, possibly with the aid of closed-loop feedback optimisation protocols.²⁷

In future work we will consider the effect on the interferometer phase of a change in detuning and Rabi frequency during the optimised pulses themselves, and extend our optimal control approach to optimise all three pulses in an interferometer sequence concurrently.

ACKNOWLEDGMENTS

The authors are grateful for funding from the UK Engineering and Physical Sciences Research Council under grant EP/T517859/1.

REFERENCES

- [1] Kasevich, M. and Chu, S., “Atomic interferometry using stimulated Raman transitions,” *Physical Review Letters* **67**(2), 181–184 (1991).
- [2] Gustavson, T. L., Bouyer, P., and Kasevich, M. A., “Precision Rotation Measurements with an Atom Interferometer Gyroscope,” *Physical Review Letters* **78**(11), 2046–2049 (1997).
- [3] Bongs, K., Holynski, M., Vovrosh, J., Bouyer, P., Condon, G., Rasel, E., Schubert, C., Schleich, W. P., and Roura, A., “Taking atom interferometric quantum sensors from the laboratory to real-world applications,” *Nature Reviews Physics* **1**(12), 731–739 (2019).
- [4] Berman, P., ed., [*Atom Interferometry*], Academic Press (1997).
- [5] Moler, K., Weiss, D. S., Kasevich, M., and Chu, S., “Theoretical analysis of velocity-selective Raman transitions,” *Physical Review A* **45**(1), 342–348 (1992).
- [6] Giese, E., “Mechanisms of matter-wave diffraction and their application to interferometers,” *Fortschritte der Physik* **63**(6), 337–410 (2015).
- [7] Cheiney, P., Fouché, L., Templier, S., Napolitano, F., Battelier, B., Bouyer, P., and Barrett, B., “Navigation-Compatible Hybrid Quantum Accelerometer Using a Kalman Filter,” *Physical Review Applied* **10**(3), 034030 (2018).
- [8] Bidet, Y., Zahzam, N., Blanchard, C., Bonnin, A., Cadoret, M., Bresson, A., Rouxel, D., and Lequentrec-Lalancette, M. F., “Absolute marine gravimetry with matter-wave interferometry,” *Nature Communications* **9**(1), 627 (2018).
- [9] Chen, Y. J., Hansen, A., Hoth, G. W., Ivanov, E., Pelle, B., Kitching, J., and Donley, E. A., “Single-Source Multiaxis Cold-Atom Interferometer in a Centimeter-Scale Cell,” *Physical Review Applied* **12**(1) (2019).

- [10] Dunning, A., Gregory, R., Bateman, J., Cooper, N., Himsforth, M., Jones, J. A., and Freegarde, T., “Composite pulses for interferometry in a thermal cold atom cloud,” *Physical Review A* **90**(3), 033608 (2014).
- [11] Gillot, P., Cheng, B., Merlet, S., and Pereira Dos Santos, F., “Limits to the symmetry of a Mach-Zehnder-type atom interferometer,” *Physical Review A* **93**(1), 013609 (2016).
- [12] Khaneja, N., Reiss, T., Kehlet, C., Schulte-Herbrüggen, T., and Glaser, S. J., “Optimal control of coupled spin dynamics: Design of NMR pulse sequences by gradient ascent algorithms,” *Journal of Magnetic Resonance* **172**(2), 296–305 (2005).
- [13] Glaser, S. J., Boscain, U., Calarco, T., Koch, C. P., Köckenberger, W., Kosloff, R., Kuprov, I., Luy, B., Schirmer, S., Schulte-Herbrüggen, T., Sugny, D., and Wilhelm, F. K., “Training Schrödinger’s cat: Quantum optimal control: Strategic report on current status, visions and goals for research in Europe,” *European Physical Journal D* **69**(12), 279 (2015).
- [14] Saywell, J. C., Kuprov, I., Goodwin, D., Carey, M., and Freegarde, T., “Optimal control of mirror pulses for cold-atom interferometry,” *Physical Review A* **98**(2), 023625 (2018).
- [15] Saywell, J., Carey, M., Belal, M., Kuprov, I., and Freegarde, T., “Optimal control of Raman pulse sequences for atom interferometry,” *Journal of Physics B: Atomic, Molecular and Optical Physics* **53**(8) (2020).
- [16] Saywell, J., Carey, M., Kuprov, I., and Freegarde, T., “Biselective pulses for large-area atom interferometry,” *Physical Review A* **101**(6), 063625 (2020).
- [17] Stoner, R., Butts, D., Kinast, J., and Timmons, B., “Analytical framework for dynamic light pulse atom interferometry at short interrogation times,” *Journal of the Optical Society of America B* **28**(10), 2418 (2011).
- [18] Feynman, R. P., Vernon, F. L., and Hellwarth, R. W., “Geometrical Representation of the Schrödinger Equation for Solving Maser Problems,” *Journal of Applied Physics* **28**(1), 49–52 (1957).
- [19] De Fouquieres, P., Schirmer, S. G., Glaser, S. J., and Kuprov, I., “Second order gradient ascent pulse engineering,” *Journal of Magnetic Resonance* **212**(2), 412–417 (2011).
- [20] Goodwin, D. L. and Kuprov, I., “Modified Newton-Raphson GRAPE methods for optimal control of spin systems,” *The Journal of Chemical Physics* **144**(20), 204107 (2016).
- [21] Hogben, H. J., Krzystyniak, M., Charnock, G. T. P., Hore, P. J., and Kuprov, I., “Spinach - A software library for simulation of spin dynamics in large spin systems,” *Journal of Magnetic Resonance* **208**(2), 179–194 (2011).
- [22] Kobzar, K., Skinner, T. E., Khaneja, N., Glaser, S. J., and Luy, B., “Exploring the limits of broadband excitation and inversion pulses,” *Journal of Magnetic Resonance* **170**(2), 236–243 (2004).
- [23] Kobzar, K., Ehni, S., Skinner, T. E., Glaser, S. J., and Luy, B., “Exploring the limits of broadband 90° and 180° universal rotation pulses,” *Journal of Magnetic Resonance* **225**, 142–160 (2012).
- [24] Saywell, J., *Optimal control of cold atoms for ultra-precise quantum sensors*, PhD thesis, University of Southampton (2020).
- [25] Skinner, T. E., Reiss, T. O., Luy, B., Khaneja, N., and Glaser, S. J., “Tailoring the optimal control cost function to a desired output: application to minimizing phase errors in short broadband excitation pulses,” *Journal of Magnetic Resonance* **172**(1), 17–23 (2005).
- [26] Bateman, J. and Freegarde, T., “Fractional adiabatic passage in two-level systems: Mirrors and beam splitters for atomic interferometry,” *Physical Review A* **76**(1), 013416 (2007).
- [27] Goodwin, D. L., Myers, W. K., Timmel, C. R., and Kuprov, I., “Feedback control optimisation of ESR experiments,” *Journal of Magnetic Resonance* **297**, 9–16 (2018).